Applied Catalysis A: General 486 (2014) 77–84

Contents lists available at ScienceDirect

Applied Catalysis A: General

journal homepage: www.elsevier.com/locate/apcata

Selective synthesis of *p*-ethylphenol by gas-phase alkylation of phenol with ethanol

M.E. Sad, H.A. Duarte, C.L. Padró, C.R. Apesteguía *

Catalysis Science and Engineering Research Group (GICIC), INCAPE – (UNL-CONICET), Santiago del Estero 2654, 3000 Santa Fe, Argentina

ARTICLE INFO

Article history:
Received 19 May 2014
Received in revised form 12 August 2014
Accepted 18 August 2014
Available online 29 August 2014

Keywords:
p-Ethylphenol
Ethylphenols
Alkylation
Phenol
Acid zeolites

ABSTRACT

The selective synthesis of *p*-ethylphenol from gas-phase alkylation of phenol with ethanol was studied on zeolites HZSM5 and HMCM22 at 523 K. Phenol reacted directly with ethanol to form ethylphenylether by O-alkylation, and *p*- and *o*-ethylphenol isomers by C-alkylation; secondary products were *m*-ethylphenol and dialkylated compounds. Both zeolites presented similar activity and formed low amounts of ethylphenylether and dialkylated products, but exhibited different ethylphenol isomers distribution. In fact, for a contact time of 99.3 g h/mol the selectivity to *p*-ethylphenol was 51.4% on HMCM22 and only 14.2% on HZSM5. The superior performance of zeolite HMCM22 for selectively producing *p*-ethylphenol was due to its narrower pore channels that suppressed the formation of dialkylated products and hampered by diffusional constraints the formation of *o*-ethylphenol. The maximum *p*-ethylphenol yield obtained on HMCM22 was 41% at a contact time of 250 g h/mol; for higher contact times, *p*-ethylphenol was increasingly converted to *m*-ethylphenol. All the samples deactivated on stream because of coke formation. The carbon amount built on HMCM22 diminished when contact time was increased thereby indicating that coke was mainly formed from the reactants. Additional catalytic runs showed that phenol was the main responsible of catalyst deactivation, probably because of its strong adsorption on surface active sites.

1. Introduction

Ethylphenols are used in the production of phenolic resins, antioxidants and in the varnish industry. *ortho*-Ethylphenol (*o*-EP) and *meta*-ethylphenol (*m*-EP) are starting materials for photochemicals while *para*-ethylphenol (*p*-EP) is employed for obtaining 4-vinylphenol, an intermediate in the synthesis of pharmaceuticals, dyes, and various antioxidants that are used in the manufacture of rubbers and polymers [1,2]. In particular, *p*-EP is conventionally prepared by sulfonation of ethylbenzene and subsequent alkali fusion of the *p*-ethylbenzene sulfonic acid obtained [2]. However this multistep process presents serious environmental concerns because of the use of strong liquid acids and sodium hydroxide at high temperatures, which cause corrosion of equipment, formation of significant amounts of sodium sulfite as byproduct and waste disposal problems. Furthermore, the boiling points of ethylphenol isomers are so close that it is impractical to separate them by distillation. The development of a novel technology using solid catalysts able to selectively promote the formation of *p*-EP is therefore highly desirable.

Few studies about ethylation of phenol on solid catalysts are found in literature and most of them deal with the synthesis of *o*-EP. Aluminum orthophosphate-alumina and BPO_4 catalysts were tested in alkylation of phenol with ethanol at 573–733 K and a mixture of O-alkylation and C-alkylation products was obtained [3,4]. Bal and Sivasanker [5] used different alkali-loaded fumed silicas with the aim of selectively producing O-alkylation products; they reported 100% of selectivity to ethylphenylether (EPE) for phenol conversions ranged from 10 to 63%. Iron catalysts such as Fe_3O_4 showed a very high selectivity to *o*-EP (97–99%) for phenol conversion of 86% at 653 K [6] whereas on CoAl-MCM-41 the *o*-EP selectivity was 80% for 40% phenol conversion at the same temperature [7]. Bezouhanova et al. [8] studied the phenol ethylation reaction on zeolites HZSM5 and Ti-HZSM5 and reported that the formation of *o*-EP was predominant at 573 K but at higher temperatures (623–723 K) the ethylphenols mixture contained mainly *p*- and *m*-EP isomers. Das and Halgeri [9] investigated the alkylation of phenol with ethanol on zeolites ZSM5 of different Si/Al ratios at 673 K with the aim of promoting the selective formation of *p*-EP; however, in all the cases, the *p*-EP yield was lower than 10%.

* Corresponding author. Tel.: +54 3424555279.
E-mail addresses: capesteg@fiq.unl.edu.ar, capesteg@gmail.com (C.R. Apesteguía).
URL: http://www.fiq.unl.edu.ar/gicic (C.R. Apesteguía).

http://dx.doi.org/10.1016/j.apcata.2014.08.016
0926-860X/

Yamagishi et al. [10] disclaimed another approach to selectively produce *p*-EP on crystalline aluminosilicates by using ethylene and phenol as reactants but the highest *p*-EP yield obtained was 8.5% for temperatures between 573 and 873 K.

In this paper we studied the gas-phase ethylation of phenol at 523 K over zeolites HZSM5 and HMCM22 with the aim of improving the selective synthesis of *p*-EP. We selected these two zeolites for performing our studies because in previous works on phenol methylation over acid zeolites we observed that HZSM5 and HMCM22 are potentially effective for promoting by shape selectivity the formation of the *para*-isomer [11,12]. Also, we decided to carry out our catalytic runs at a mild temperature taken into account that the production of *m*-EP, the most thermodynamically stable isomer, is favored at higher temperatures. Results will show that at 523 K and contact time of 250 g mol/h, the *p*-EP yield on zeolite HMCM22 was 41% that is significantly higher than the best values reported in literature.

2. Experimental

2.1. Catalyst preparation

Commercial zeolite HZSM5 (Zeocat Pentasil PZ-2/54, Si/Al = 20, 0.43% Na) was calcined at 723 K in dry air flow (60 cm^3/min) during 3 h before use. Zeolite HMCM22 was synthesized according to [13], by using sodium aluminate (Alfa Aesar, Technical Grade), silica (Aerosil Degussa 380), sodium hydroxide (Merck, >99%), hexamethyleneimine (Aldrich, 99%) and deionized water as reagents. The molar composition of the synthesis gel was $SiO_2/Al_2O_3 = 30$, $OH/SiO_2 = 0.18$, hexamethyleneimine/$SiO_2 = 0.35$ and $H_2O/SiO_2 = 45$. The gel was stirred at 423 K in a Teflon lined stainless steel autoclave. After crystallization, the solid was recovered by centrifugation, washed thoroughly with distilled water, dried at 373 K and finally calcined at 773 K in dry air (60 cm^3/min).

2.2. Catalyst characterization

The crystal structure of HMCM22 was determined by powder X-ray diffraction methods (XRD) using a Shimadzu XD-D1 diffractometer and Ni-filtered CuKα radiation. XRD patterns were recorded in the 2θ range from 2° to 45°. Total surface areas (S_{BET}) and sample porosities were measured by N_2 physisorption at its normal boiling point in an Autosorb Quantochrome Instrument 1-C sorptometer. The zeolite micropore volumes were determined using the adsorption branch of nitrogen isotherms by both Dubinin–Radushkevich [14] and *t*-plot [15] methods. The *t*-plot was obtained by using de Harkins–Jura Eq. [16]. The external surface areas (S_e), were obtained from the slopes of the *t*-plot lines. Before adsorption, samples were treated under vacuum at 623 K for 8 h.

The nature, density and strength of surface acid sites were determined by infrared spectroscopy (IR) in a Shimadzu FTIR Prestige-21 spectrophotometer using pyridine as probe molecule. Samples were ground to a fine powder and pressed into wafers (10–30 mg). The discs were mounted in a quartz sample holder and transferred to an inverted T-shaped Pyrex cell equipped with CaF_2 windows. Samples were initially outgassed in vacuum at 723 K during 2 h and then a background spectrum was recorded after being cooled down to room temperature. Spectra were recorded at room temperature, after admission of pyridine, and sequential evacuation at 298, 423, and 573 K.

Coke formed on the catalysts during reaction was measured by temperature programmed oxidation (TPO) using a 2% O_2/N_2 molar stream. After reaction, the samples were maintained at the reaction temperature in N_2 flow 1 h before to perform the TPO experiment, in order to eliminate weakly adsorbed molecules of reactants or products. Samples (30–50 mg) were heated at 10 K/min from 298 K to 1073 K. The evolved CO_2 was converted into methane in a fixed bed reactor containing a methanation catalyst (Ni/kieselguhr) at 673 K. Then, methane was analyzed using a flame ionization detector (gas chromatograph: SRI 8610C).

2.3. Catalyst testing

The alkylation of phenol (Merck, >99%) with ethanol (Merck, 99.8%) in gas phase was carried out in a fixed bed tubular reactor at 523 K and 101.3 kPa in continuous flow of N_2. Samples (particles with 0.35–0.42 mm diameter) were pretreated in situ, at 723 K in air flow (90 cm^3/min) for 2 h before reaction. Liquid reactants (ethanol (*E*) and phenol (*P*), *E*/*P* = 1:1 molar) were fed using a syringe pump and vaporized at 473 K in N_2 (75 cm^3/min). Catalytic experiments were performed at different contact times (W/F_P^0), between 24.8 and 300 g h/mol. Samples were collected every 20 min during 3 h. Reactant and product concentrations were measured by gas chromatography using an Agilent 6850 chromatograph equipped with a 30-m HP-Chiral capillary column (inner diameter: 0.32 mm, film thickness: 0.5 μm) connected to a flame ionization detector. Phenol (X_P) and ethanol (X_E) conversions were calculated as: $X_{P,E} = (Y_{P,E}^0 - Y_{P,E})/Y_{P,E}^0$ where Y_P^0 and Y_E^0 are the molar fractions of phenol and ethanol at the entrance of the reactor while Y_P and Y_E are the molar fractions of phenol and ethanol at the exit. Main products of the phenol ethylation reaction were *p*-EP, *m*-EP, *o*-EP and EPE; two other minor chromatographic peaks were also detected, probably corresponding to dialkylated ethylphenols that are named here as DAP. In order to perform carbon balance calculations, we used as chromatographic response factor for these two compounds the average response factor determined experimentally for 2,4 and 2,6 xylenols in a previous work [12]. The selectivity to product *i* formed from phenol (S_i, mol of product *i*/mol of phenol reacted) was determined as: $S_i = [Y_i/\Sigma Y_i]$ where Y_i is the molar fraction of products formed from phenol. Diethylether and ethylene formed from ethanol were also detected. Selectivities to these products (mol of diethylether or ethylene/mol of ethanol reacted) were determined as: $S_{\text{diethylether}} = Y_{\text{diethylether}} * 2/(Y_E^0 - Y_E)$ and $S_{\text{ethylene}} = Y_{\text{ethylene}}/(Y_E^0 - Y_E)$ where $Y_{\text{diethylether}}$ and Y_{ethylene} are the molar fractions of both products at the exit of the reactor.

3. Results and discussion

3.1. Catalyst characterization

The physical and textural properties of the samples are presented in Table 1. BET surface areas of HZSM5 and HMCM22 were similar (350–400 m^2/g) as well as the corresponding external surface areas (about 70 m^2/g). The zeolite micropore volumes (<20 Å) were determined analyzing the adsorption branch of nitrogen isotherms by both Dubinin–Radushkevich and *t*-plot methods. Although the values obtained by Dubinin–Radushkevich method were slightly higher than those determined from *t*-plots (Table 1), both methods revealed that the micropore volume of HMCM22 was higher than that of HZSM5. In the case of zeolite HMCM22, it was observed two linear ranges in *t*-plot (not shown here). The first linear range did not pass by the origin which indicated the presence of ultramicropores (<6 Å), most likely the zeolite micropores (4.0 × 5.5 Å and 4.0 × 5.0 Å). Therefore, we also determined the ultramicropore volume of HMCM22 (0.10 cm^3/g). The pore volume determined here for HMCM22 is consistent with values reported in literature. For example, the micropore volumes determined by Rigoreau et al. [17] and by Juttu and Lobo [18] using *t*-plots were 0.193 and 0.2 cm^3/g, respectively. In particular, the micropore and

Table 1
Textural properties of the catalysts.

Catalysts	S_{BET} (m^2/g)	Pore size (Å)	*t*-Plot method			Dubinin–Radushkevich method
			Micropore volumen (cm^3/g)	Ultramicropore volume (cm^3/g)	External surface area, S_e (m^2/g)	Micropore volumen (cm^3/g)
HZSM5	350	5.1 × 5.5; 5.3 × 5.6	0.155	–	73	0.18
HMCM22	400	4.0 × 5.5; 4.1 × 5.1	0.169	0.10	68	0.21

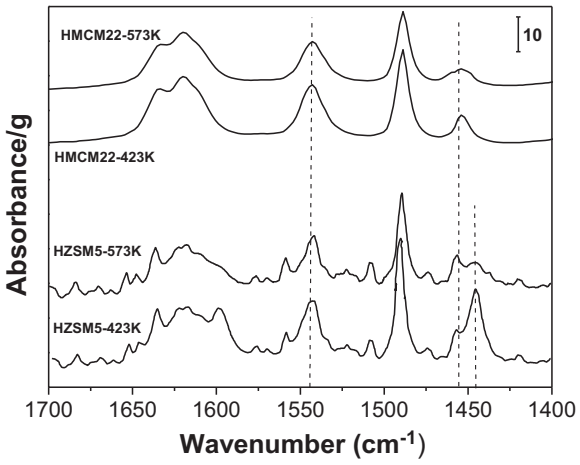

Fig. 1. FTIR spectra of pyridine adsorbed at 298 K and evacuated at 423 K and 573 K on zeolites HMCM22 and HZSM5.

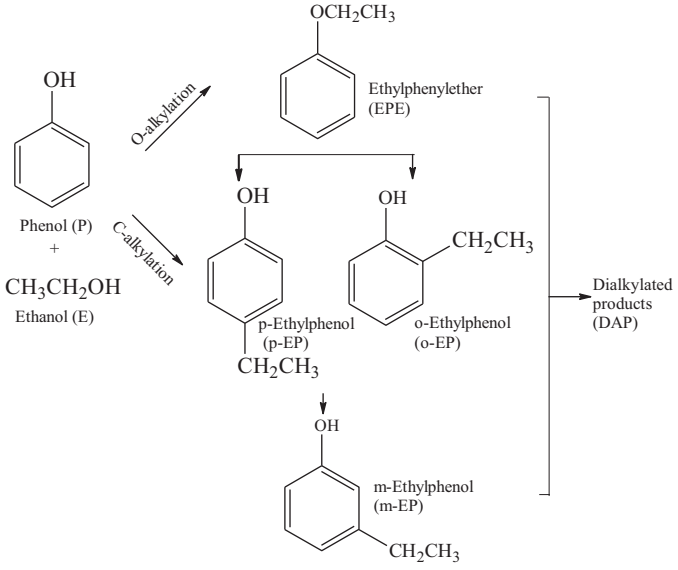

Scheme 1. Reaction network for the alkylation of phenol with ethanol.

ultramicropore volumes reported by Meloni et al. [19] for a zeolite HMCM22 were 0.195 and 0.137 cm^3/g, respectively.

The nature and strength of surface acid sites were determined from the IR spectra of adsorbed pyridine after admission at 298 K and sequential evacuation at 423 and 573 K (Fig. 1). The relative contributions of Lewis (*L*) and Brønsted (*B*) acid sites were obtained by deconvolution and integration of pyridine absorption bands at around 1540 cm^{-1} and between 1440 cm^{-1} and 1460 cm^{-1}, respectively [20–23]; results are presented in Table 2. Fig. 1 shows that the 1440–1460 cm^{-1} band in the IR spectrum obtained on HZSM5 after evacuation at 423 K was split in two overlapping peaks corresponding to pyridine adsorbed on Al (1455 cm^{-1}) and Na (1445 cm^{-1}) Lewis acid sites. The total amount of surface acid sites determined on HZSM5 after evacuation at 423 K was similar to that on HMCM22 (Table 2). Nevertheless, the acid site distribution was different; in fact, the *B*/*L* ratio on HMCM22 was three times higher than on HZSM5. In order to evaluate the acid site strength, we compared the amounts of pyridine remaining on the catalyst surface following evacuations at 423 and 573 K. From data of Table 2 we determined that the Py-573 K/Py-423 K ratio (i.e. the ratio of total amounts of pyridine remaining on the sample after evacuation at 573 K and 423 K) was 0.77 and 0.65 on HMCM22 and HZSM5, respectively. These results showing that significant amounts of pyridine remain adsorbed on the catalyst surface after evacuation at 573 K, revealed that both zeolites contain strong acid sites. On the other hand, the *B*/*L* ratio determined on HZSM5 after evacuation at 423 K (*B*/*L* = 1.0) increased up to 1.8 following evacuation at 523 K, which suggests that Brønsted sites present stronger acidity than Lewis sites. Furthermore, comparison of IR spectra obtained on HZSM5 after evacuation at 423 K and 573 K allows inferring that Na Lewis acid sites (peak at 1445 cm^{-1}) are weaker than Al Lewis acid sites (peak at 1455 cm^{-1}). On HMCM22 the *B*/*L* ratio also increased with the evacuation temperature, from 3.2 (evacuation at 423 K) to 3.7 (evacuation at 573 K).

3.2. Catalytic tests

3.2.1. Alkylation of phenol with ethanol: catalyst activity

The gas-phase phenol ethylation was carried out on HZSM5 and HMCM22 at 523 K using an equimolar reactant ratio and identical contact time. Fig. 2 shows the evolution of phenol and ethanol conversions (X_P, X_E) and selectivities (S_i) as a function of time on stream. Main products from phenol ethylation were *ortho*, *meta* and *para* ethylphenols (EP) formed by C-alkylation of phenol, EPE (O-alkylation of phenol) and dialkylated products (diethyphenols and ethyl–ethylphenyl ether). Diethylether, ethylene and C_{3+} alkenes formed from ethanol conversion reactions were also detected. Results obtained in previous works [12,24] for phenol methylation allow us to propose the reaction network of Scheme 1 for the ethylation of phenol on solid acids. Phenol can initially react with ethanol via two parallel alkylation reactions to form primary products: by O-alkylation phenol is transformed to EPE and by C-alkylation yields directly *o*-EP and *p*-EP. Then EPE may be converted to ethylphenols while isomerization of *o*-EP and *p*-EP leads to the formation of *m*-EP. Finally, ethylphenols can react with ethanol to produce dialkylated products.

Fig. 2 shows that the initial phenol and ethanol conversions were similar on HZSM5 and HMCM22 ($X_P^0 \cong 40\%$, $X_E^0 = 100\%$). As expected, ethanol conversion was higher than phenol conversion because ethanol not only reacts with phenol but also is consumed in parallel dehydration/condensation reactions. Both X_P and X_E diminished with time-on-stream reflecting the in situ sample deactivation. Initially, the reaction formed on both zeolites essentially ethylphenols and dialkylated products and minor amounts of EPE, but with the progress of the reaction the EPE selectivity increased at the expense of EP and DAP. After 3 h reaction the EPE selectivity on HZSM5 increased up to 36% while S_{EP} decreased from 92% to

Table 2
Characterization of catalyst acidity by FTIR of pyridine.

Catalysts	Evacuation temperature[a]					
	T = 423 K			T = 573 K		
	Lewis sites (L), area/g	Brønsted sites (B), area/g	B/L	Lewis sites (L), area/g	Brønsted sites (B), area/g	B/L
HZSM5	341	337	1.0	155	287	1.8
HMCM22	176	560	3.2	120	444	3.7

[a] Pyridine preadsorbed at 298 K.

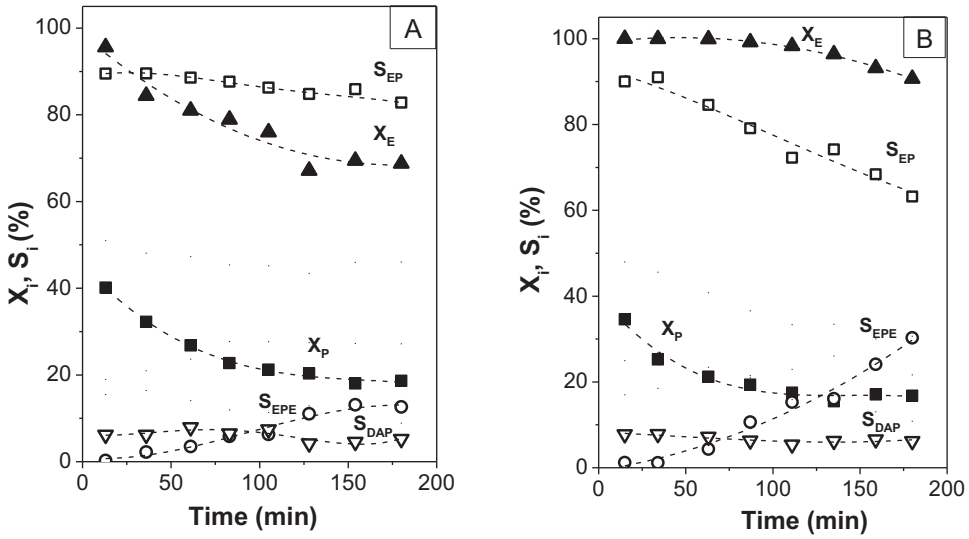

Fig. 2. Conversions (X_i) and selectivities (S_i) as a function of time on stream. A: HMCM22, B: HZSM5 [523 K, P_T = 101.3 kPa, $P_P = P_E$ = 1.1 kPa, W/F_P = 99.3 g h/mol].

65%. In contrast, on HMCM22, S_{EPE} was only 10% at the end of the run and S_{EP} decreased slightly from 90% to 83%.

The alkylation of aromatic compounds with ethanol on zeolites occurs through an electrophilic substitution on the aromatic ring by the alkylating agent formed from ethanol dehydration on zeolite acid sites [25]. In our case, ethanol is dehydrated on zeolitic OH groups forming surface-bound ethoxide species that can alkylate phenol or produce ethylene (by intramolecular dehydration) and diethylether (by dehydration/condensation). Based on previous works [26–29], we present in Scheme 2 the mechanisms of ethanol conversion on BrØnsted acid sites to produce ethylphenols, ethylene or diethylether via the formation of surface-bound ethoxide intermediates. The alkylating agent attacks the phenol ring by electrophilic substitution in *ortho* and *para* positions because of the electron donor effect of phenol OH group that increases the electronic density of positions 2, 4, and 6 in the ring.

Previous studies have reported that the selectivity of ethanol dehydration to ethylene and diethylether over zeolites depends on the sample topology, acidity and reaction temperature [30–32]. Here we have carried out a brief study of ethanol conversion reactions on HZSM5 and HMCM22 at 473 and 523 K. Results are presented in Table 3. At 473 K, the initial ethanol conversion was higher on HMCM22 ($X_E^0 = 70\%$) than on HZSM5 ($X_E^0 = 56\%$); both zeolites formed essentially diethylether. At 523 K, ethanol was totally converted on HMCM22 and HZSM5, producing mainly ethylene. This selectivity change with the reaction temperature is consistent with previous studies reporting that the activation energy of the ethanol dehydration to ethylene is higher than that of ethanol conversion to diethylether [32]. Both zeolites produced significant amounts of additional products at 573 K (Table 3, $X^0_{\text{Others}} \cong 16\%$), probably C_{3+} hydrocarbons formed from ethylene as reported in literature [33].

In summary, from the catalyst activity data obtained at 523 K and presented in Fig. 2 and Table 3 we infer that zeolites HMCM22 and HZSM5 present similar initial activity for phenol ethylation and convert totally ethanol.

3.2.2. Alkylation of phenol with ethanol: catalyst selectivity

Table 4 presents the values of initial reactant conversions determined from Fig. 2 as well as of the initial selectivities to all the products formed from phenol ethylation reaction. On both zeolites the carbon balance was higher than 90%, the selectivity to DAP lower than 9% and EPE formation negligible. In contrast, the ethylphenol product distribution observed on HMCM22 was significantly different to that obtained on HZSM5. In fact, on HMCM22 the main product was *p*-EP ($S^0_{p\text{-EP}} = 51.4\%$) giving a *para*/(*ortho* + *meta*) isomer ratio of 1.5 while HZSM5 formed mostly *o*-EP ($S^0_{o\text{-EP}} = 49.0\%$) so that the *para*/(*ortho* + *meta*) ratio was only 0.2. Based on these results that show the superior performance of HMCM22 for selectively promoting the formation of *p*-EP, we selected this zeolite to perform additional catalytic runs with the aim of gaining insight on the phenol ethylation mechanism and exploring the possibility of increasing the *p*-EP yield (the initial *p*-EP yield on HMCM22 as determined from data of Table 4 was about 22%, at 523 K and W/F_P = 99.3 g h/mol).

3.2.3. p-Ethylphenol synthesis

Additional catalytic runs were carried out on HMCM22 by varying the contact time between 24.8 and 250 g h/mol. The observed catalyst deactivation, however, required that each data point be obtained on fresh catalyst and that initial yields be obtained by extrapolating to initial time on stream. Fig. 3 shows the evolution of initial reactant conversions and yields as a function of contact time. The local slopes of the yield curves in Fig. 3 give the rate of formation of each product at a specific reactant conversion and contact time. The nonzero initial slopes of *p*-EP, *o*-EP and EPE

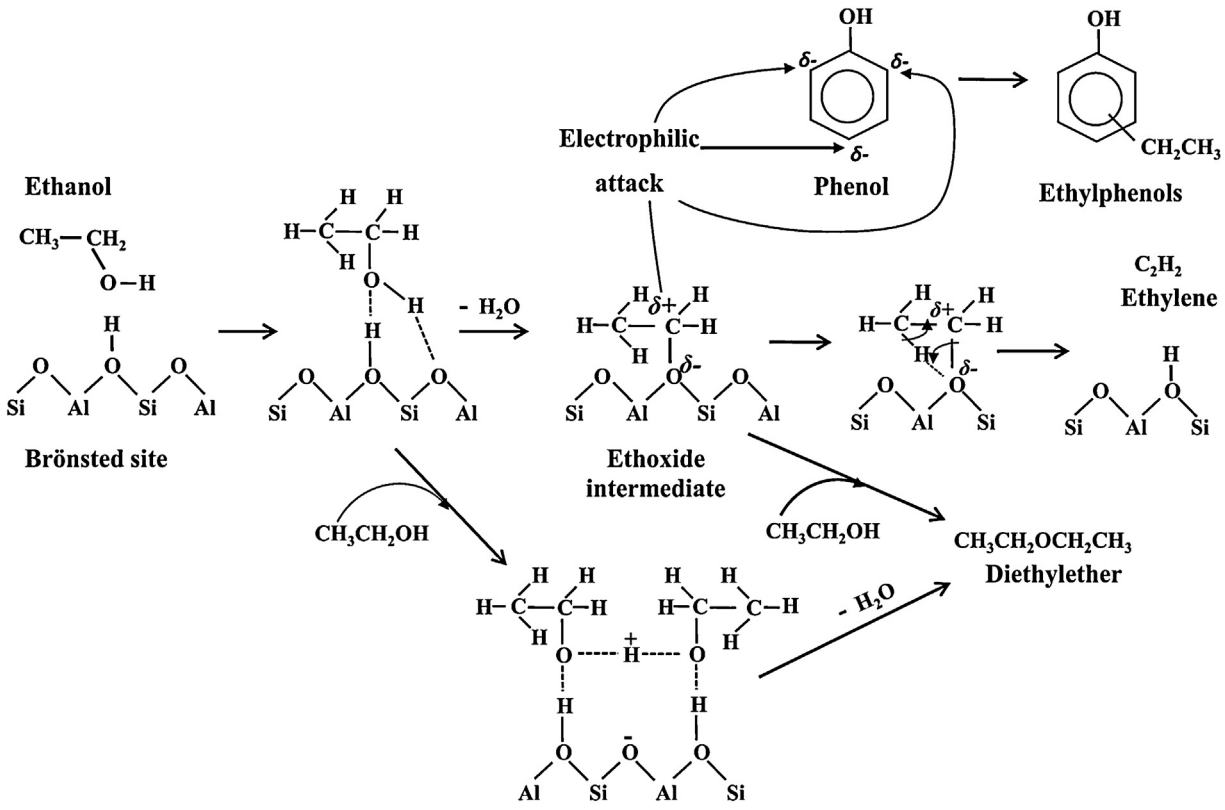

Scheme 2. Ethanol conversion mechanisms via the formation of surface-bound ethoxide intermediate: phenol alkylation, dehydration to ethylene and dehydration/condensation to diethylether.

Table 3
Ethanol conversion reactions on zeolites HZSM5 and HMCM22.

Temperature (K)	HZSM5				HMCM22			
	X_E^0 (%)	$S^0_{ethylene}$ (%)	$S^0_{diethylether}$ (%)	S^0_{others} (%)	X_E^0 (%)	$S^0_{ethylene}$ (%)	$S^0_{diethylether}$ (%)	S^0_{others} (%)
473	56	11	87	2	70	6	91	3
523	100	80	3	17	100	80	4	16

Ethanol conversion and selectivities obtained at $t = 0$.
101.3 kPa total pressure, P_E = 1.1 kPa, W/F_E = 99.3 g h/mol.

Table 4
Catalytic results for the alkylation of phenol with ethanol.

Catalyst	Initial conversions (%)		Initial selectivities (%)					C balance (%)
	X_P^0	X_E^0	$S^0_{p\text{-EP}}$	$S^0_{o\text{-EP}}$	$S^0_{m\text{-EP}}$	S^0_{EPE}	S^0_{DAP}	
HZSM5	40.2	100	14.2	49.0	22.8	1.0	7.1	94.1
HMCM22	42.6	99	51.4	15.9	15.2	1.1	8.3	91.9

523 K, 101.3 kPa total pressure, $P_P = P_E$ = 1.1 kPa, W/F_P = 99.3 g h/mol.

confirm that they are primary products formed directly by the attack of ethanol to phenol as depicted in Scheme 1. In contrast, the zero initial slopes obtained for *m*-EP and DAP yield curves suggest that these compounds are secondary products. *m*-EP is probably formed by isomerization of *p*-EP and *o*-EP while the consecutive alkylation of ethylphenols with another ethanol molecule accounts for the production of dialkylated products. On the other hand, Fig. 3 shows that the EPE yield curve reaches a maximum at $W/F_P \cong 49.6$ g h/mol, indicating that EPE is converted to secondary products, probably ethylphenols, with increasing contact time. All these results are consistent with the phenol ethylation reaction network proposed in Scheme 1.

The higher selectivity to *p*-EP obtained on HMCM22 in comparison to HZSM5 (Table 4) may now be analyzed in terms of the shape selectivity concept and taking into account the reaction pathways involved in Scheme 1. Zeolite HZSM5 has a tridimensional structure with 10-MR straight channel (5.1 Å × 5.5 Å) interconnected to sinusoidal 10-MR channel (5.3 Å × 5.6 Å). HMCM22 has a particular pore structure with two independent pore systems. One pore system is tridimensional and composed of 12-MR supercages (18.2 Å × 7.12 Å × 7.1 Å) connected by 10MR windows (4.0 Å × 5.5 Å); the second, bidimensional, is composed of interconnected sinusoidal 10MR channels (4.0 Å × 5.0 Å) and does not contain any cages [34,35]. The narrower channels of zeolite HMCM22 can change the product distribution of phenol ethylation reaction according to the ease of diffusivity of product molecules. Although HMCM22 contain 12-MR supercages, only molecules that can diffuse through the 10-MR pores may reach the internal active

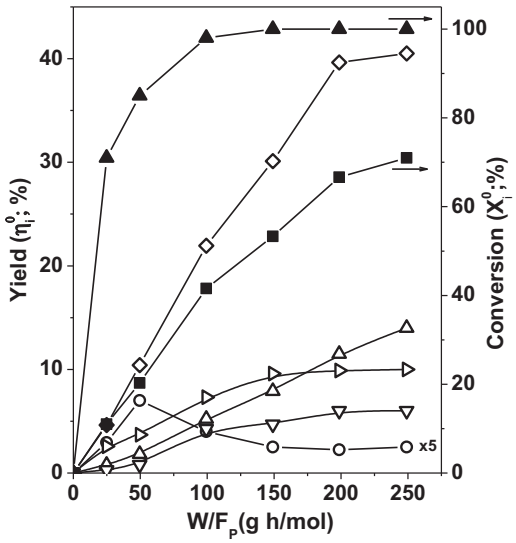

Fig. 3. Conversions and yields at $t = 0$ as a function of contact time on HMCM22. Phenol (■), ethanol (▲), *p*-EP (◊), *o*-EP (▷), *m*-EP (△), EPE (○), DAP (▽) [523 K, P_T = 101.3 kPa, $P_P = P_E$ = 1.1 kPa].

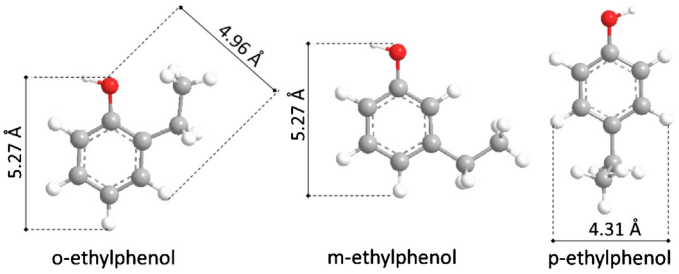

Fig. 4. Ethylphenol isomers dimensions.

sites of this zeolite because the 12-MR supercages are connected to the exterior through a 10-MR window. Catalytic results in Table 4 prove that phenol can go inside the channels of zeolites HZSM5 and HMCM22 and form ethylphenols. However, the initial selectivity to *p*-EP was clearly higher on HMCM22 ($S^0_{p\text{-EP}} = 51.4\%$) than on HZSM5 ($S^0_{p\text{-EP}} = 14.2\%$). This result probably reflects the fact that inside the HMCM22 pores the *o*-EP isomer would diffuse at much smaller rates than *p*-EP because its bigger dimension (Fig. 4 shows the relative dimensions of ethylphenol isomers). There are not specific data in literature about the diffusion coefficients of ethylphenol isomers on HMCM22, but several authors have studied the gas-phase diffusion of xylene isomers on 10-member ring zeolites. Roque-Malherbe et al. [36] determined that the intrinsic diffusion coefficient of *o*-xylene at 300 K is about four orders of magnitude lower on HMCM22 than on HBEA. On zeolite HZSM11, it was reported that the *p*-xylene diffusion coefficient at 400–425 K is 20–30 times higher than that of *o*-xylene [37], while on HZSM5 at 373 K the same comparison of diffusion coefficients reached a difference of two orders of magnitude [38]. A similar qualitative difference of the transport rates of *p*-EP and *o*-EP into the 10-MR pores of HMCM22 may explain the drastic *para*-selectivity improvement observed in Table 4 for the ethylation of phenol on HMCM22 as compared to HZSM5.

Fig. 3 shows that X^0_p increased with W/F_P on HMCM22, reaching 71% at W/F_P = 250 g h/mol; ethanol was totally converted for contact times higher than 99.3 g h/mol. *p*-EP yield continuously increased with contact time up to 41% ($S^0_{p\text{-EP}} = 59\%$) for W/F_P = 250 g h/mol. In contrast, *o*-EP yield reached about 10% at W/F_P = 149 g h/mol and

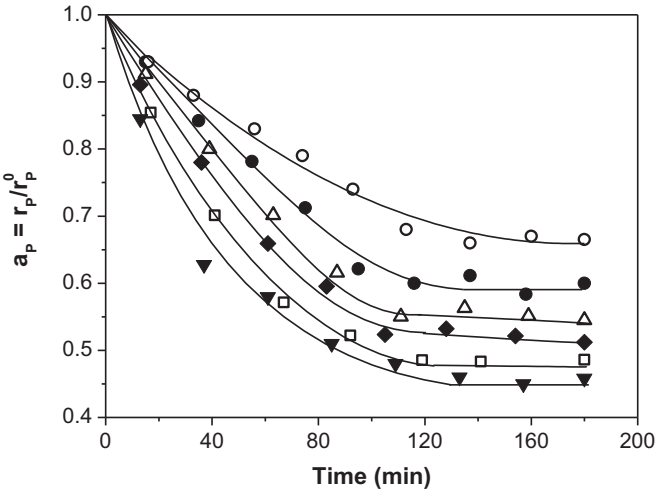

Fig. 5. Time evolution of the activity for phenol conversion (a_P) on HMCM22 for different contact times. (○) 250.0 g h/mol; (●) 198.6 g h/mol; (△) 149.0 g h/mol; (♦) 99.3 g h/mol; (□) 49.6 g h/mol; (▼) 24.8 g h/mol [523 K, P_T = 101.3 kPa, $P_P = P_E$ = 1.1 kPa].

then remained almost constant for higher W/F_P values. Thus, the *p*-EP/*o*-EP molar ratio increased up to about 4 at W/F_P = 250 g h/mol, thereby confirming that zeolite HMCM22 markedly improves the selective formation of *p*-EP. Nevertheless, the *m*-EP yield constantly increased with W/F_P reflecting the *m*-EP formation from isomerization of *p*- and *o*-EP isomers; $\eta^0_{m\text{-EP}}$ reached 14% for W/F_P = 250 g h/mol. Production of DAP was very low over the entire W/F_P range and η^0_{DAP} did not exceed 6%. This late result indicates that the narrow channels of HMCM22 hinder the formation of bulky intermediates involved in the alkylation of ethylphenols to DAP. The EPE yield was negligible (less than 1%) for W/F_P higher than 99.3 g h/mol which reveals that this primary product of phenol ethylation is rapidly converted to secondary products.

In summary, results in Fig. 3 show that on HMCM22, at 523 K and W/F_P = 250 g h/mol, phenol conversion reaches 71% yielding 41% of *p*-EP. This $\eta^0_{p\text{-EP}}$ value is significantly higher than those reported in previous (few) papers that investigated the selective production of *p*-EP by phenol ethylation [9,10]. The superior performance of zeolite HMCM22 for selectively producing *p*-EP is due to its narrow pore channels that not only suppresses the alkylation of ethylphenols to dialkylated products but also hamper by diffusional constraints the formation of *o*-EP. Nevertheless, the maximum *p*-EP yield was obtained here at W/F_P = 250 g h/mol; when W/F_P higher than 250 g h/mol were employed the $\eta^0_{p\text{-EP}}$ diminished because *p*-EP was increasingly converted to *m*-EP. The isomerization of *p*-EP to *m*-EP is favored on HMCM22 because this zeolite contains a high concentration of strong Brønsted acid sites (Table 2).

On the other hand, the activity decay on HMCM22 during the progress of the reaction was considerable in all the catalytic tests performed in this work (see Fig. 2), thereby suggesting that the reactions forming coke intermediates were not suppressed to any significant extent. In basis of this observation, and taking into account that no previous studies exist regarding catalyst deactivation during the phenol ethylation reaction, we decided to carry out additional catalytic tests in order to gain insight on catalyst activity decay and coke formation.

3.2.4. Catalyst deactivation and coke formation

To obtain a better knowledge about the activity decay observed on zeolite HMCM22 for phenol ethylation, we plotted in Fig. 5 the evolution of the activity for the conversion of phenol (a_P) as a function of time for different contact times. The activity a_P is defined

Table 5
Deactivation results for phenol ethylation.

Contact time, W/F_P (g h/mol)	Phenol conversion, X_P^0 (%)	Deactivation results	
		d_0 (h^{-1})[a]	C (%)[b]
24.8	11.0	0.69	7.2
49.6	21.0	0.63	6.5
99.3	42.6	0.50	4.8
149.0	55.1	0.47	3.6
198.6	66.7	0.29	1.7
250.0	71.0	0.19	1.1

HMCM22, 523 K, P_T = 101.3 kPa, $P_P = P_E$ = 1.1 kPa.
[a] Initial deactivation, $d_0 = (da/dt)_{t=0}$.
[b] Carbon formed after the 3 h runs.

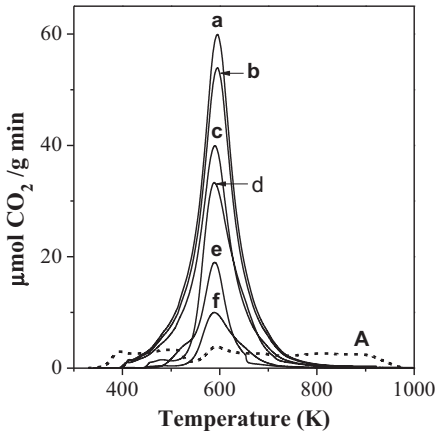

Fig. 6. TPO profiles of HMCM22 samples recovered after using in 3-h phenol ethylation runs at different contact times: (a) 24.8 g h/mol; (b) 49.6 g h/mol; (c) 99.3 g h/mol; (d) 149.0 g h/mol; (e) 198.6 g h/mol; (f) 250.0 g h/mol [523 K, P_T = 101.3 kPa, $P_P = P_E$ = 1.1 kPa]. TPO profile A: HMCM22 sample recovered after using in 3-h ethanol conversion run [523 K, 99.3 g h/mol, P_T = 101.3 kPa, P_E = 1.1 kPa].

as $a_P = r_P/r_P^0$, where r_P^0 and r_P are the phenol conversion rates at $t = 0$ and $t = t$, respectively. Fig. 5 shows that the catalyst activity decay clearly diminished when W/F_P was increased. In order to quantitatively evaluate the effect that varying contact time W/F_P (and consequently X_P^0) has on phenol conversion rate decay, we determined from the a_P vs t curves of Fig. 5 the parameter $d_0 = -[da_P/dt]_{t=0}$ accounting for initial deactivation rate [39]. Results given in Table 5 show that d_0 diminished from 0.69 h^{-1} to 0.19 h^{-1} when W/F_P was increased from 24.8 g h/mol to 250 g h/mol.

The observed sample deactivation on stream could be attributed to the formation of carbonaceous deposits from consecutive or parallel reactions of reactants and products on surface active sites. We characterized the carbon deposited on the samples recovered from the catalytic experiments showed in Fig. 5 by temperature-programmed oxidation technique. Before the TPO characterization, samples were treated at 523 K in N_2 during 60 min. The obtained TPO curves are presented in Fig. 6. The shapes of TPO curves were similar for all the samples, presenting a single combustion peak with a maximum at about 570 K. Carbon contents were determined from the areas under the curves of Fig. 6 and are included in Table 5. The formation of coke on HMCM22 diminished from 7.2% C (for W/F_P = 24.8 g h/mol) to 1.1% C (for W/F_P = 250.0 g h/mol). Data in Table 5 show that initial deactivation rate d_0 increased proportionally with the %C deposited on the samples, thereby suggesting that coke formation was responsible for the activity decay observed in Fig. 5 by blocking the surface active sites.

According to Table 5, phenol conversion increases while initial deactivation d_0 and % coke diminish when contact time is increased. This result strongly suggests that deactivation of zeolite HMCM22 on stream is mainly related to the presence of the reactants, ethanol and/or phenol. Therefore, we decide to investigate the formation of coke over HMCM22 when only ethanol is feeding to the reactor at the same operation conditions used for the phenol ethylation reaction in Fig. 2 (523 K, W/F_P = 99.3 g h/mol, P_E = 1.1 kPa, reaction length = 3 h). We analyzed the ethanol conversion products (the initial product composition is included in Table 3) and determined the amount of carbon formed on HMCM22 at the end of the run by TPO technique. Although ethanol conversion remained close to 100% during the entire catalytic run, we observed the change of color of zeolite HMCM22 after reaction which indicated the presence of surface carbonaceous deposits. The TPO curve obtained for HMCM22 sample recovered after the 3-h ethanol conversion run consisted of a broad band with several peaks of CO_2 evolved between 350 and 980 K (Fig. 6, curve A). Thus, ethanol conversion via dehydration, dehydrogenation and condensation reactions proceeding mainly on Brønsted acid sites (Scheme 2) forms also surface carbonaceous deposits on HMCM22. Nevertheless, Fig. 6 shows that the profile of curve A was completely different as compared to those obtained from samples recovered after phenol ethylation runs (TPO profiles a–f). Furthermore, the %C determined by integration of TPO curve A was 2.1%, significantly lower than the amount of carbon obtained on HMCM22 sample recovered after the phenol ethylation run carried out under the same operation conditions (4.8%, Table 5). All these results strongly suggested that phenol is the main responsible for coke formation in phenol ethylation, either because of its strong adsorption on catalyst active sites or by forming coke precursors via secondary reactions with ethanol-derived species. In a previous work on phenol methylation [40] we characterized by infrared spectroscopy the nature of coke formed on stream and detected the presence of phenolate, aromatic and polyaromatic species adsorbed mainly on Lewis acid sites. Taking into account that phenol is adsorbed preferentially on Lewis acid centers, predominantly in vertical orientation [41,42], formation of coke intermediates on Lewis acid sites would suppress the active sites required to promote phenol ethylation and may explain the catalyst activity decay on stream observed in this work.

4. Conclusions

Zeolites HZSM5 and HMCM22 promote efficiently the gas-phase ethylation of phenol producing mainly ethylphenols and lower amounts of ethylphenylether and diethylphenols. Zeolite HMCM22 is particularly suitable to selectively produce *p*-ethylphenol because its sinusoidal 10-member ring channel structure hinders by shape selectivity the formation of *o*-ethylphenol and blocks the production of dialkylated products. At 523 K and 71% of phenol conversion, the HMCM22 zeolite yields 41% of *p*-ethylphenol; for higher phenol conversion values the *p*-ethylphenol yield diminishes because *p*-ethylphenol is increasingly converted to *m*-ethylphenol.

The activity of zeolite HMCM22 for phenol ethylation declines with time on stream due to coking and the deactivation rate increases proportionally to the amount of carbon deposited on the solid. Formation of carbon decreases with phenol conversion because coke is formed essentially from ethanol/phenol reactants. Ethanol forms surface carbonaceous deposits on HMCM22 conversion via dehydration, dehydrogenation and condensation reactions. Nevertheless, phenol is the main responsible for coke formation in phenol ethylation, either because of its strong adsorption on catalyst active sites or by forming coke precursors via secondary reactions with ethanol-derived species.

Acknowledgements

We thank the Universidad Nacional del Litoral (UNL), the Agencia Nacional de Promoción Científica y Tecnológica (ANPCyT) and the Consejo Nacional de Investigaciones Científicas y Técnicas(CONICET), Argentina, for the financial support of this work.

References

[1] V.A. Knop, L.A. Pilato, Phenolic Resins. Chemistry, Applications and Performance, Springer, Berlin, 1985.
[2] Ullman's Encyclopedia of Industrial Chemistry, 7th ed., Willey-VCH, 2011.
[3] J. Mercy, J.M. Marinas, J.V. Sinisterra, React. Kinet. Catal. Lett. 22 (1983) 175–180.
[4] S. Esteban Santos, J.M. Marinas Rubio, M.P. Martinez Alcazar, React. Kinet. Catal. Lett. 24 (1984) 247–251.
[5] R. Bal, S. Sivasanker, Appl. Catal. A: Gen. 246 (2003) 373–382.
[6] H. Grabowska, J. Wrzyszcz, Res. Chem. Intermed. 17 (1992) 263–270.
[7] A. Vinu, M. Karthik, M. Miyahara, V. Murugesan, K. Ariga, J. Mol. Catal. A: Chem. 230 (2005) 151–157.
[8] C. Bezouhanova, M.A. Al-Zihari, H. Lechert, React. Kinet. Catal. Lett. 46 (1992) 153–158.
[9] J. Das, A.B. Halgeri, Appl. Catal. A: Gen. 194–195 (2000) 359–363.
[10] T. Yamagishi, T. Idai, E. Takaliash, US Patent 4,927,979, Maruzen Petrochemical Co., 1990.
[11] M.E. Sad, C.L. Padró, C.R. Apesteguía, Appl. Catal. A 342 (2008) 40–48.
[12] M.E. Sad, C.L. Padró, C.R. Apesteguía, Catal. Today 133–135 (2008) 720–728.
[13] M.K. Rubin, P. Chu, US Patent 4,954,325, 1990.
[14] M.M. Dubinin, L.V. Radushkevich, Dokl. Akad. Nauk SSSR 55 (1947) 331–337.
[15] B.C. Lippens, B.G. Linsen, J.H. De Boer, J. Catal. 3 (1964) 32–37.
[16] W.D. Harkins, G. Jura, J. Chem. Phys. 11 (1943) 431–432.
[17] J. Rigoreau, S. Laforge, N.S. Gnep, M. Guisnet, J. Catal. 236 (2005) 45–54.
[18] G.G. Juttu, R.F. Lobo, Microporous Mesoporous Mater. 40 (2000) 9–23.
[19] D. Meloni, S. Laforge, D. Martin, M. Guisnet, E. Rombi, V. Solinas, Appl. Catal. A: Gen. 215 (2001) 55–66.
[20] E.P. Parry, J. Catal. 2 (1963) 371–379.
[21] J.W. Ward, J. Catal. 10 (1968) 34–46.
[22] H. Knözinger, Adv. Catal. 25 (1976) 184–271.
[23] G. Busca, Catal. Today 41 (1998) 191–200.
[24] M.E. Sad, C.L. Padró, C.R. Apesteguía, J. Mol. Catal. A: Chem. 327 (2010) 63–72.
[25] A. Corma, F.J. Llopis, C. Martinez, G. Sastre, S. Valencia, J. Catal. 268 (2009) 9–17.
[26] W. Wang, J. Jiao, Y.J. Jiang, S.S. Ray, M. Hunger, Chemphyschem 6 (2005) 1467–1469.
[27] J.N. Kondo, K. Ito, E. Yoda, F. Wakabayashi, K. Domen, J. Phys. Chem. B 109 (2005) 10969–10972.
[28] E.G. Derouane, J.B. Nagy, P. Dejaifve, J.H.C. van Hooff, B.P. Spekman, J.C. Vedrine, C. Naccache, J. Catal. 53 (1978) 40–55.
[29] C.B. Phillips, R. Datta, Ind. Eng. Chem. Res. 36 (1997) 4466–4475.
[30] C. de las Pozas, R. Lopez-Cordero, J.A. Gonzalez-Morales, N. Travieso, R. Roque-Malherbe, J. Mol. Catal. 83 (1993) 145–156.
[31] H. Chiang, A. Bhan, J. Catal. 271 (2010) 251–261.
[32] H. Xin, X. Li, Y. Fang, X. Yi, W. Hua, Y. Chu, F. Zhang, A. Zheng, H. Zhang, X. Li, J. Catal. 312 (2014) 204–215.
[33] F. Ferreira Madeira, N.S. Gnep, P. Magnoux, S. Maury, N. Cadran, Appl. Catal. A: Gen. 367 (2009) 39–46.
[34] S.L. Lawton, A.S. Fung, G.J. Kennedy, L.B. Alemany, C.D. Chang, G.H. Hatzikos, D.N. Lissy, M.K. Rubin, H.K.C. Timken, S. Steuernagel, D.E. Woesner, J. Phys. Chem. 100 (1996) 3788–3798.
[35] M.E. Leonowicz, J.A. Lawton, S.L. Lawton, M.K. Rubin, Science 264 (1994) 1910–1913.
[36] R. Roque-Malherbe, R. Wendelbo, A. Mifsud, A. Corma, J. Phys. Chem. 99 (1995).
[37] R. Roque-Malherbe, V. Ivanov, Microporous Mesoporous Mater. 47 (2001) 25–38.
[38] G. Mirth, J. Cejka, J.A. Lercher, J. Catal. 139 (1993) 24–33.
[39] C.L. Padró, C.R. Apesteguía, J. Catal. 226 (2004) 308–320.
[40] M.E. Sad, C.L. Padró, C.R. Apesteguía, Appl. Catal. A: Gen. 475 (2014) 305–313.
[41] K.V.R. Chary, K. Ramesh, G. Vidyasagar, V.V. Rao, J. Mol. Catal. A: Chem. 198 (2003) 195–204.
[42] K. Tanabe, T. Nishizaki, in: G.C. Bond, P.B. Wells, F.C. Tompkins (Eds.), Proceedings of the Sixth International Conference on Catalysis, vol. 2, The Chemical Society, London, 1977, p. 863.